Measurements of Quasiparticle Tunneling Dynamics in a Band-Gap-Engineered Transmon Qubit

L. Sun,[1] L. DiCarlo,[1,2] M. D. Reed,[1] G. Catelani,[1] Lev S. Bishop,[1,3] D. I. Schuster,[1,4] B. R. Johnson,[1,5] Ge A. Yang,[1,4]
L. Frunzio,[1] L. Glazman,[1] M. H. Devoret,[1] and R. J. Schoelkopf[1]

[1]*Department of Physics and Applied Physics, Yale University, New Haven, Connecticut 06520, USA*
[2]*Kavli Institute of Nanoscience, Delft University of Technology, Delft, The Netherlands*
[3]*Joint Quantum Institute and Condensed Matter Theory Center, Department of Physics, University of Maryland,
College Park, Maryland 20742, USA*
[4]*Department of Physics and James Franck Institute, University of Chicago, Chicago, Illinois 60637, USA*
[5]*Raytheon BBN Technologies, Cambridge, Massachusetts 02138, USA*
(Received 11 December 2011; published 8 June 2012)

We have engineered the band gap profile of transmon qubits by combining oxygen-doped Al for tunnel junction electrodes and clean Al as quasiparticle traps to investigate energy relaxation due to quasiparticle tunneling. The relaxation time T_1 of the qubits is shown to be insensitive to this band gap engineering. Operating at relatively low-E_J/E_C makes the transmon transition frequency distinctly dependent on the charge parity, allowing us to detect the quasiparticles tunneling across the qubit junction. Quasiparticle kinetics have been studied by monitoring the frequency switching due to even-odd parity change in real time. It shows the switching time is faster than 10 μs, indicating quasiparticle-induced relaxation has to be reduced to achieve T_1 much longer than 100 μs.

Quantum information processing based on superconducting qubits has made tremendous progress toward realizing a practical quantum computer in the last few years [1–3]. However, the coherence times of superconducting qubits still need to improve to reach the error correction threshold. For example, the single-qubit gate error rate is limited by qubit decoherence [4–6]. Understanding decoherence mechanisms, in particular those responsible for qubit relaxation, is therefore crucial. Quasiparticles have received significant attention recently as one such possible limiting factor [7–9]. At low temperatures, thermal-equilibrium quasiparticles should be irrelevant because their density is exponentially suppressed. In practice, however, nonequilibrium quasiparticles are present from unknown sources [10,11]. The key question is then whether these nonequilibrium quasiparticles are currently limiting qubit relaxation and, if not, what limit they will ultimately impose. The answer will be relevant to all superconducting qubits.

Quasiparticles in qubit electrodes do not themselves cause significant qubit decoherence. Instead, it is the dissipative and incoherent tunneling of quasiparticles across a Josephson junction that leads to decoherence [12]. The tunneling process is characterized by the quasiparticle current spectral density $S_{qp}(\omega)$. The low frequency component in $S_{qp}(\omega)$ can cause dephasing, but this dephasing channel can be eliminated by reducing the qubit's sensitivity to charge noise, as in flux [13,14], phase [15], and transmon [16] qubits. The high frequency component will cause energy relaxation in all types of superconducting qubits. A transmon qubit has the energy level structure shown in Fig. 1(a). Quasiparticle tunneling causes both

qubit relaxation and odd-even parity switching, with rates $\Gamma_{1\to0}^{qp} = |M_{01}|^2 S_{qp}(\omega_{01})$ and $\Gamma_{oe,i}^{qp} = |M_{oe,i}|^2 S_{qp}(\delta_i)$ respectively, where $\omega_{01}/2\pi$ is the qubit ground-to-excited transition frequency, $\delta_i/2\pi$ is the odd-to-even transition frequency for state $i = 0, 1$, and M_{01} and $M_{oe,i}$ are the matrix elements describing the interaction between the qubit and quasiparticles [12].

The dynamics of quasiparticle tunneling in single-Cooper-pair transistors (SCPTs) and Cooper-pair box qubits have been studied extensively, although the understanding is still incomplete. The measured odd-even parity switching time falls in a large range from the order of 1 μs to the order of 1 ms [10,17–20], or possibly even longer in some cases [21–23] that have no observable quasiparticle "poisoning." One way to suppress quasiparticle tunneling is to engineer the band gap profile near the tunnel junction [10,17–21]. This band gap engineering technique has been shown to be effective in extending the parity switching time dramatically from 1 μs to above 1 ms [20].

In this Letter, we employ band gap engineering for the first time in transmon qubits, in an attempt to make the odd-even parity switching time in the measurable range >100 μs, which would then eliminate quasiparticles as a source of decoherence. We measure the qubit relaxation time T_1 as a function of temperature of transmon qubits, which have significantly different band gaps. At low temperatures, the saturation of T_1 of both transmons at approximately the same level suggests a mechanism other than thermal quasiparticles for qubit relaxation. To investigate if nonequilibrium quasiparticles are limiting T_1, we then study the quasiparticle kinetics in a band gap–engineered transmon operated in the low-E_J/E_C regime,

where E_J and E_C are the Josephson and the charging energy, respectively. Qubit spectroscopy shows two qubit transition frequencies associated with the even- and odd-charge states, demonstrating the presence and tunneling of quasiparticles across the qubit junction. This indicates that, with our design, nonequilibrium quasiparticles have not been removed by band gap engineering, contrary to the results of experiments in SCPTs [10,18,20]. We study the ground-state parity switching rate $\Gamma_{oe}^{qp} \equiv \Gamma_{oe,0}^{qp}$ in the time domain finding $1/\Gamma_{oe}^{qp} < 10~\mu$s. For typical device parameters, the expected ratio of parity switching rate to quasiparticle-induced qubit relaxation rate, $\Gamma_{oe}^{qp}/\Gamma_{1\to0}^{qp} \sim$ 10–100 [12]. Therefore, while we cannot establish quasiparticle tunneling as the dominant source of energy relaxation in our devices, our bound indicates that reducing the quasiparticle-induced decay rate will be necessary to achieve T_1 much longer than 100 μs.

Our transmon qubits are measured using a coplanar waveguide cavity in a conventional circuit-quantum-electrodynamics architecture [24]. All devices are measured in a cryogen-free dilution refrigerator with a 20 mK base temperature. Oxygen-doped Al, which has an energy gap $\Delta \approx 280~\mu$eV ($T_c \approx 1.9$ K) about 60% higher than clean Al ($\Delta \approx 180~\mu$eV, $T_c \approx 1.2$ K), is used as the electrodes of Josephson tunnel junctions deposited by standard double-angle evaporation [25]. The oxygen dopants are introduced with a continuous O_2 flow during the Al deposition. The same technique has also been used in SCPTs to realize a large band gap [10,18]. To create quasiparticle traps, a third layer of clean Al is deposited to cover the whole oxygen-doped Al layers to within $\sim$100 nm from the junctions [Fig. 1(b)]. Figure 1(c) shows the expected band gap profile near the junction. This profile is expected to trap quasiparticles away from the

tunnel junction. The energy gaps of oxygen-doped layers are determined by independent T_c measurements (not shown) of thin films evaporated under the same nominal conditions as for the tunnel junction.

However, our band gap engineering does not appear to affect T_1 (see Table I in Supplemental Material [26] for a list of devices). A comparison of T_1 as a function of temperature for two representative devices is shown in Fig. 2(a): one qubit is fabricated with clean Al only and the other with oxygen-doped Al without the third layer quasiparticle trap. The decrease of T_1 with temperatures above 150 mK for the red curve and 250 mK for the blue curve, respectively, indicates the effect of thermally generated quasiparticles [6,12]. The higher corner temperature confirms that oxygen-doped Al indeed has a larger energy gap. The saturation of T_1 at low temperatures for both clean and oxygen-doped Al devices at the same value indicates that thermal quasiparticles are not limiting T_1. Figure 2(b) shows the saturated T_1 as a function of frequency for four qubits, each of which has its own flux bias line allowing individual tuning of the qubit frequency [2], fabricated with both oxygen-doped Al and quasiparticle traps described earlier. The qubit lifetimes are limited to a quality factor $Q \sim 65,000$, similar to previously reported T_1 on qubits fabricated with clean Al only [27].

Nonequilibrium quasiparticles have been observed in the band gap–engineered devices, as will be shown later, so here we will only focus on the effect on T_1 from those nonequilibrium quasiparticles. The lack of qualitative
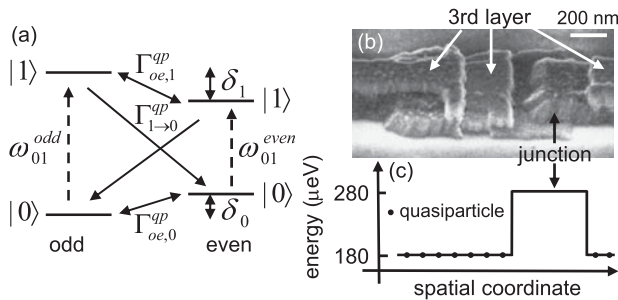

FIG. 1. (a) Low energy–level structure of a transmon qubit. The parity state with larger separation between $|0\rangle$ and $|1\rangle$ qubit states is assigned to odd without loss of generality. δ_0 and δ_1: Energy difference between odd-even parities for the ground and first excited state, respectively, $\delta_1 \gg \delta_0$. $\omega_{01}^{odd} - \omega_{01}^{even} = \omega_{oe} \approx \delta_1$ is the charge dispersion. $\Gamma_{oe,i}^{qp}$ is the switching rate between qubit states of different parities. $\Gamma_{1o\to0e}^{qp} \approx \Gamma_{1e\to0o}^{qp} = \Gamma_{1\to0}^{qp}$ is the qubit relaxation rate because $\omega_{01}^{odd} \approx \omega_{01}^{even} = \omega_{01} \gg \delta_1$. (b) SEM image of a typical device fabricated by three-angle evaporation to engineer the band gap profile. (c) Expected band gap profile near the tunnel junction.
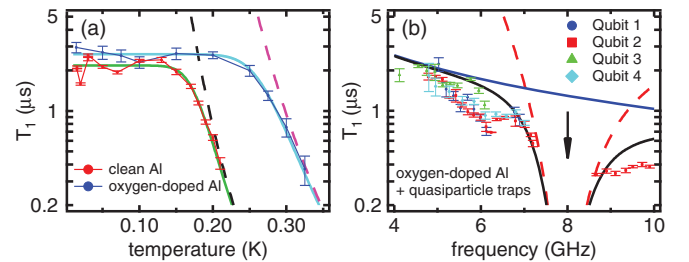

FIG. 2 (color online). (a) Measured qubit relaxation time T_1 as a function of temperature for two transmon qubits: one qubit is fabricated with clean Al only with a transition frequency $f_{01} = 4.25$ GHz and the other with oxygen-doped Al, but without the third layer of quasiparticle traps, with $f_{01} = 5.16$ GHz. The device layout is identical to Fig. 1(a) in Ref. [1]. Dashed black and magenta lines are theory for relaxation due to thermal quasiparticles, assuming $\Delta \approx 180$ and 280 μeV, respectively [8]. The solid green and cyan lines represent the sum of the theoretical expectations for thermal-equilibrium quasiparticles and the best-fit saturated T_1. (b) T_1 vs frequency on qubits fabricated with oxygen-doped Al and quasiparticle traps. The device layout is identical to Fig. 1(a) in Ref. [2]. Dashed red line: Purcell-induced relaxation time; solid blue line: $Q = 65,000$; solid black line: a combination of the Purcell effect and a constant Q. Neither oxygen-doped Al nor quasiparticle traps improve T_1 qualitatively. The black arrow indicates the cavity frequency.

improvements of T_1 suggests three possible scenarios: T_1 is not limited by nonequilibrium quasiparticles, the quasiparticle contribution to T_1 has not been affected by our band gap engineering, or both. In any case, we wish to find the quasiparticle-induced qubit relaxation rate $\Gamma_{1\to0}^{qp}$. However, this rate cannot be measured directly in the presence of other sources of relaxation, so we instead measure the dynamics of quasiparticle tunneling Γ_{oe}^{qp} in the time domain, from which we can estimate $\Gamma_{1\to0}^{qp}$ [12]. In order to measure Γ_{oe}^{qp}, we operate the transmon qubit in the low-E_J/E_C regime where the qubit spectrum will have two distinct parities caused by quasiparticle tunneling across the junction. Thus, Γ_{oe}^{qp} can be studied by monitoring the dynamics of one particular parity in real time.

We have fabricated a single transmon qubit with both oxygen-doped Al and quasiparticle traps, and we operate it at $E_J/E_C \approx 12.5$ by tuning the qubit frequency to $f_{01} \approx 4.5$ GHz, where $T_1 = 2$ μs. To protect the qubit from spontaneous emission [27] through the low-Q cavity ($Q = 500$), a Purcell filter is also integrated on the chip. The device layout is identical to Fig. 1(a) in Ref. [28]. At this large detuning from the cavity frequency $f_c = 8.072$ GHz, a direct readout of the qubit state is difficult because of the weak dispersive interaction between the qubit and the cavity. Instead, to enhance readout fidelity, the qubit is pulsed to $f_{01} \approx 7$ GHz prior to measurement. By making use of the high-power Jaynes-Cummings readout [29], we achieve a single-shot fidelity $F = 42\%$.

The presence and tunneling of nonequilibrium quasiparticles is demonstrated by the clearly observed "eye" pattern in the qubit spectroscopy as a function of gate-induced charge n_g [Fig. 3(a)] [11]. The two peaks in Fig. 3(b) have almost equal height, implying no preferred parity, and

both parity switching times τ_o (odd-to-even) and τ_e (even-to-odd) are shorter than the 50 ms averaging time at each pixel.

To study the dynamics of quasiparticle tunneling, a selective π pulse is applied repeatedly every 10 μs at one of two parity frequencies (for simplicity, we choose the odd parity frequency for all data presented here), immediately followed by a measurement of the qubit state [Fig. 4(a)]. This selective π pulse will excite the qubit only when the parity is odd. We note that, due to the smallness of δ_0 [Fig. 1(a)], the selective π pulse will also cover the transition $|0, \text{even}\rangle$ to $|1, \text{odd}\rangle$, but for nondegenerate quasiparticles the probability of this unwanted transition is small compared to that of the direct photon transition $|0, \text{odd}\rangle$ to $|1, \text{odd}\rangle$. Thus, by interrogating the qubit state after the π pulse, the qubit parity can be inferred. To ensure that the qubit begins in the ground state and that the qubit frequency has stabilized after the rapid tuning from 7 to 4.5 GHz at the beginning of each experimental cycle, the repetition rate is set to $t_s = 10$ μs $= 5T_1$. As shown in Ref. [20], if slow quasiparticle tunneling dynamics of the order of 1 ms could be achieved in our band gap–engineered transmon qubits, the presented method would easily resolve these dynamics, thus completely ruling out quasiparticles as a source of qubit relaxation.

Because quasiparticles tunnel across the qubit junction randomly, a random telegraph signal (RTS) is expected. To overcome low single-shot readout fidelity, we perform a Fourier transform of the time domain data to study the power spectral density (PSD) to better extract the RTS information. Background charge motion limits the experiment duration, since the qubit frequency shifts noticeably every few minutes. In total, 12 million measurements are recorded and Fourier-transformed.

The stability of the readout is particularly important for this measurement. Thus, to minimize the drift during the experiment, the readout result is digitized by thresholding the measurement results [Fig. 4(b)]. From each
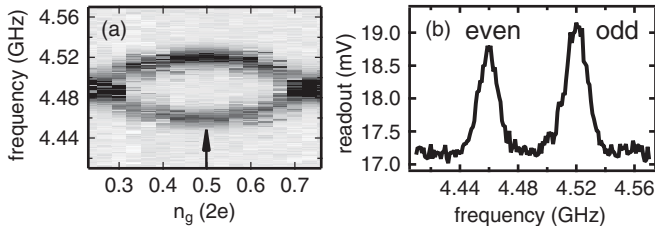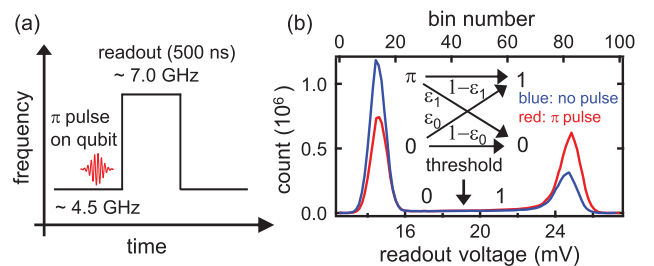

FIG. 3. (a) Spectroscopy of a qubit with engineered band gap as a function of gate-induced charge n_g. The gate voltage is applied to the qubit through a bias tee at the cavity input port. For each pixel, a Gaussian pulse ($\sigma = 20$ ns, corresponding to a π pulse on resonance) is applied at the indicated frequency and the qubit is immediately measured. Each pixel is an average of 5000 repetitions (50 ms). Darker pixels correspond to higher homodyne readout voltages that are proportional to the probability of the qubit in the excited state. An "eye"-shaped pattern indicates charge-e jumps associated with the tunneling of nonequilibrium quasiparticles. (b) Cross section of (a) at $n_g = 0.5$ as indicated by the black arrow in (a). The charge dispersion is 60 MHz. We refer to the lower (upper) frequency branch as the even (odd) parity peak.

FIG. 4 (color online). (a) Schematic of the measurement. A selective π pulse is applied to one of the two parity peaks in Fig. 3, followed by an immediate readout of the qubit state at about 7 GHz, where readout fidelity is improved. Lines: The flux pulse sequence. The process is repeated every 10 μs. (b) Histogram of the readout at the odd parity peak in Fig. 3(b). A threshold $V_{th} = 19$ mV is chosen to digitize the readout. Inset: Schematic of an imperfect readout with false positives (negatives) ϵ_0 (ϵ_1).

measurement, one bit of information is extracted. False positives ϵ_0 and negatives ϵ_1 of the readout [Fig. 4(b) inset] will reduce the RTS amplitude. Note that, due to the switching of the qubit between the two parities, ϵ_0 and ϵ_1 cannot be extracted directly from Fig. 4(b), but they can easily be obtained by combining histograms of the readout at the even parity peak in Fig. 3(b) (see Supplemental Material [26] for details). We find $\epsilon_0 \approx \epsilon_1 = 0.29$, as well as the probability of the qubit at the odd parity $P_{\text{odd}} = 56\%$. Thus the readout fidelity is $F = 1 - \epsilon_0 - \epsilon_1 \approx 42\%$.

We first test the sensitivity of the experiment to fluctuations of parity by applying a "π mask" to the measurement system to imitate the success and failure of a π pulse on the qubit. The π mask, generated by a field-programmable gate array (FPGA), is a pseudorandom control sequence that enables or disables a π pulse applied to the qubit immediately prior to readout. It generates an RTS with a specified time constant $\tau_\pi = \tau_{\pi 0} + \tau_{\pi 1}$ and a 50% duty cycle ($\tau_{\pi 0} = \tau_{\pi 1}$). If the parity switches fast compared to τ_π (as will be confirmed later), the RTS amplitude in the readout is reduced to $A_{\text{con}} = P_{\text{odd}}F$ due to the parity duty cycle and the finite readout fidelity [Fig. 5(a) inset; also see Supplemental Material [26]]. Figure 5(a) shows the PSDs of the control experiments with a π mask with different time constants $\tau_\pi = 2$ ms, 600 μs, 200 μs, 108 μs, and 72 μs, respectively. All measured PSDs agree very well with theory (see Supplemental Material [26] for details).

We now turn to the measurement of the parity switching rate $\Gamma_{\text{oe}}^{\text{qp}}$ of the qubit, showing in Fig. 5(b) the PSD obtained without the π mask. The measured spectrum is almost flat and white noise–like, suggesting fast qubit parity switching. An upper bound can be placed on $\Gamma_{\text{oe}}^{\text{qp}}$ by comparing with the theoretical predictions for the observed duty cycle $P_{\text{odd}} = \tau_o/(\tau_o + \tau_e) = 56\%$ and different time constants, τ_o and τ_e. We note that the theoretical predictions in Fig. 5(b) assume an RTS amplitude $A = F$, almost twice as large as that in the control experiment, because the RTS is just from parity switching (see the Supplemental Material [26]). Even at $\tau_{\text{oe}} = \tau_o + \tau_e = 20$ μs, there is still some deviation of the theoretical prediction from data. We infer from this that qubit parity switching time is faster than our repetition time, $\tau_o \sim \tau_e < 10$ μs. This upper bound has been lowered by more than three orders of magnitude from the previous estimate in Ref. [11]. In Fig. 5(b), there is a small rise in the spectrum below ~ 1 kHz, but its amplitude is an order of magnitude smaller than the theoretical prediction at $\tau_{\text{oe}} = 2$ ms with the same corner frequency, excluding quasiparticle tunneling as the cause. A slow background charge motion can contribute to this low-frequency plateau. An analysis of the spectrum down to 0.1 Hz with the absence of a Lorentzian plateau [Fig. 5(b) inset] confirms that no slow RTS process is missed.

The upper bound of $\tau_o \sim \tau_e < 10$ μs places an upper bound on the quasiparticle-induced qubit relaxation time
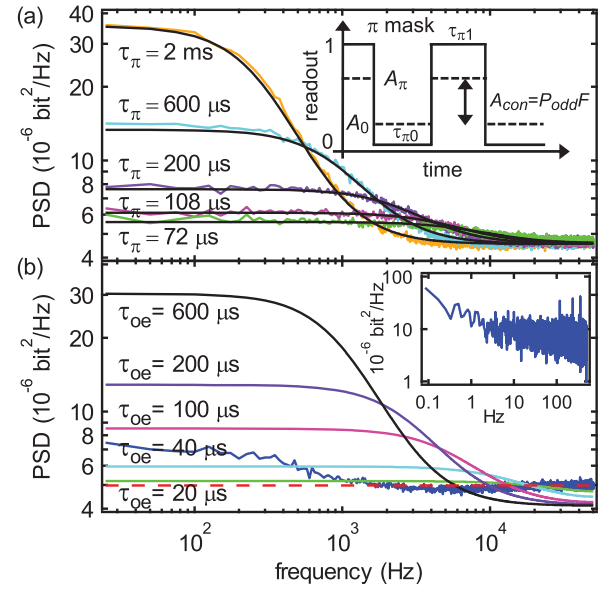

FIG. 5 (color online).   (a) Power spectral densities of control experiments using a π mask with different time constants $\tau_\pi = \tau_{\pi 0} + \tau_{\pi 1}$. $\tau_{\pi 0} = \tau_{\pi 1}$ are the time constants associated with the π mask. The color curves are data and black curves are theoretical predictions. Inset: Schematic of the control experiment with a π mask, an RTS with specified time constants and generated by an FPGA. The expected RTS amplitude is reduced to $A_{\text{con}} = A_\pi - A_0 = P_{\text{odd}}F$, where A_π and A_0 are the statistical averages of the readout during the π mask assuming parity switches fast compared to τ_π, P_{odd} is the probability of the qubit to be in the odd parity state, and F is the readout fidelity. (b) Measured PSDs and theoretical predictions for the direct experiment on $\Gamma_{\text{oe}}^{\text{qp}}$ without the π mask. Blue curve is the measured Fourier spectrum and the color curves are theoretical predictions for different qubit parity switching times $\tau_{oe} = \tau_o + \tau_e$, where τ_o and τ_e are the odd-to-even and even-to-odd switching times, respectively. The red dashed line is the white-noise spectrum in the limit τ_o, $\tau_e < t_s$, the sampling time. The near absence of any deviation from white noise at high frequencies indicates τ_o, $\tau_e < 10$ μs. Inset: The PSD at low frequency does not show a Lorentzian plateau.

$1/\Gamma_{1\to 0}^{\text{qp}}$. Recent theory [12] predicts that the quasiparticle-induced qubit decay rate is much slower than the even-odd parity switching rate. For current device parameters, $\Gamma_{\text{oe}}^{\text{qp}} \approx 1/\tau_o$ and $\Gamma_{\text{oe}}^{\text{qp}}/\Gamma_{1\to 0}^{\text{qp}} \sim 30$, implying a qubit relaxation time $1/\Gamma_{1\to 0}^{\text{qp}} < 300$ μs. Combining this ratio with the measured $T_1 = 2$ μs gives a lower bound $\tau_o \sim \tau_e > 100$ ns. These results do not allow us to determine whether quasiparticles dominate the energy relaxation of current transmon qubits. However, it is evident that quasiparticle tunneling will need to be reduced in order to extend T_1 beyond ~ 100 μs.

We have engineered the band gap profile of transmon qubits by combining oxygen-doped Al for tunnel junction electrodes and clean Al as quasiparticle traps in an attempt to reduce the qubit relaxation due to quasiparticles. However, the measured qubit relaxation time is found to be insensitive to the size of the superconducting gap and

to quasiparticle traps. On the other hand, the nondegradation of the qubit relaxation time suggests no measurable change of the junction quality from oxygen-doped Al. Nonequilibrium quasiparticles leading to the charge-parity switching have been observed in all devices. Moreover, the quasiparticle-induced parity switching is shown to be faster than 10 μs, an upper bound limited by the detection bandwidth. This fast parity switching rate, different from the results of other experiments in SCPTs, could be due to three things. First, the size of the transmon electrodes is much larger and the quasiparticle density may depend on the electrode size. Second, the qubit readout might generate quasiparticles or stimulate the tunneling of quasiparticles between electrodes. A third possibility is that the interface between the oxygen-doped and clean Al layers might not be transparent enough. Although our results neither prove nor disprove that nonequilibrium quasiparticles limit T_1 in transmon qubits, it does indicate that quasiparticle-induced energy relaxation must be reduced in the future to achieve T_1 much longer than 100 μs. Future experiments could be able to resolve quasiparticle tunneling dynamics by increasing the experimental repetition rate through either the use of a fast reset [28] or by artificially limiting the qubit T_1 through other means, such as the Purcell effect.

[1] L. DiCarlo, J. M. Chow, J. M. Gambetta, L. S. Bishop, B. R. Johnson, D. I. Schuster, J. Majer, A. Blais, L. Frunzio, S. M. Girvin, et al., Nature (London) **460,** 240 (2009).

[2] L. DiCarlo, M. D. Reed, L. Sun, B. R. Johnson, J. M. Chow, J. M. Gambetta, L. Frunzio, S. M. Girvin, M. H. Devoret, and R. J. Schoelkopf, Nature (London) **467,** 574 (2010).

[3] M. Neeley, R. C. Bialczak, M. Lenander, E. Lucero, M. Mariantoni, A. D. O'Connell, D. Sank, H. Wang, M. Weides, J. Wenner, et al., Nature (London) **467,** 570 (2010).

[4] E. Lucero, M. Hofheinz, M. Ansmann, R. C. Bialczak, N. Katz, M. Neeley, A. D. O'Connell, H. Wang, A. N. Cleland, and J. M. Martinis, Phys. Rev. Lett. **100,** 247001 (2008).

[5] J. M. Chow, J. M. Gambetta, L. Tornberg, J. Koch, L. S. Bishop, A. A. Houck, B. R. Johnson, L. Frunzio, S. M. Girvin, and R. J. Schoelkopf, Phys. Rev. Lett. **102,** 090502 (2009).

[6] H. Paik, D. I. Schuster, L. S. Bishop, G. Kirchmair, G. Catelani, A. P. Sears, B. R. Johnson, M. J. Reagor,

L. Frunzio, L. Glazman, et al., Phys. Rev. Lett. **107,** 240501 (2011).

[7] J. M. Martinis, M. Ansmann, and J. Aumentado, Phys. Rev. Lett. **103,** 097002 (2009).

[8] G. Catelani, J. Koch, L. Frunzio, R. J. Schoelkopf, M. H. Devoret, and L. I. Glazman, Phys. Rev. Lett. **106,** 077002 (2011).

[9] M. Lenander, H. Wang, R. C. Bialczak, E. Lucero, M. Mariantoni, M. Neeley, A. D. O'Connell, D. Sank, M. Weides, J. Wenner, et al., Phys. Rev. B **84,** 024501 (2011).

[10] J. Aumentado, M. W. Keller, J. M. Martinis, and M. H. Devoret, Phys. Rev. Lett. **92,** 066802 (2004).

[11] J. A. Schreier, A. A. Houck, J. Koch, D. I. Schuster, B. R. Johnson, J. M. Chow, J. M. Gambetta, J. Majer, L. Frunzio, M. H. Devoret, et al., Phys. Rev. B **77,** 180502 (2008).

[12] G. Catelani, R. J. Schoelkopf, M. H. Devoret, and L. I. Glazman, Phys. Rev. B **84,** 064517 (2011).

[13] J. R. Friedman, V. Patel, W. Chen, S. K. Tolpygo, and J. E. Lukens, Nature (London) **406,** 43 (2000).

[14] C. H. van der Wal, A. C. J. ter Haar, F. K. Wilhelm, R. N. Schouten, C. J. P. M. Harmans, T. P. Orlando, S. Lloyd, and J. E. Mooij, Science **290,** 773 (2000).

[15] J. M. Martinis, S. Nam, J. Aumentado, and C. Urbina, Phys. Rev. Lett. **89,** 117901 (2002).

[16] J. Koch, T. M. Yu, J. M. Gambetta, A. A. Houck, D. I. Schuster, J. Majer, A. Blais, M. H. Devoret, S. M. Girvin, and R. J. Schoelkopf, Phys. Rev. A **76,** 042319 (2007).

[17] A. J. Ferguson, N. A. Court, F. E. Hudson, and R. G. Clark, Phys. Rev. Lett. **97,** 106603 (2006).

[18] O. Naaman and J. Aumentado, Phys. Rev. B **73,** 172504 (2006).

[19] M. D. Shaw, R. M. Lutchyn, P. Delsing, and P. M. Echternach, Phys. Rev. B **78,** 024503 (2008).

[20] N. A. Court, A. J. Ferguson, R. Lutchyn, and R. G. Clark, Phys. Rev. B **77,** 100501 (2008).

[21] P. Joyez, P. Lafarge, A. Filipe, D. Esteve, and M. H. Devoret, Phys. Rev. Lett. **72,** 2458 (1994).

[22] A. Amar, D. Song, C. J. Lobb, and F. C. Wellstood, Phys. Rev. Lett. **72,** 3234 (1994).

[23] V. Bouchiat, D. Vion, P. Joyez, D. Esteve, and M. H. Devoret, Phys. Scr. **T76,** 165 (1998).

[24] A. Wallraff, D. I. Schuster, A. Blais, L. Frunzio, R.-S. Huang, J. Majer, S. Kumar, S. M. Girvin, and R. J. Schoelkopf, Nature (London) **431,** 162 (2004).

[25] G. J. Dolan, Appl. Phys. Lett. **31,** 337 (1977).

[26] See Supplemental Material at http://link.aps.org/supplemental/10.1103/PhysRevLett.108.230509 for measured devices, extraction of parameters from histograms, and spectrum of an RTS with finite readout fidelity.

[27] A. A. Houck, J. A. Schreier, B. R. Johnson, J. M. Chow, J. Koch, J. M. Gambetta, D. I. Schuster, L. Frunzio, M. H. Devoret, and S. M. Girvin et al., Phys. Rev. Lett. **101,** 080502 (2008).

[28] M. D. Reed, B. R. Johnson, A. A. Houck, L. DiCarlo, J. M. Chow, D. I. Schuster, L. Frunzio, and R. J. Schoelkopf, Appl. Phys. Lett. **96,** 203110 (2010).

[29] M. D. Reed, L. DiCarlo, B. R. Johnson, L. Sun, D. I. Schuster, L. Frunzio, and R. J. Schoelkopf, Phys. Rev. Lett. **105,** 173601 (2010).